Received 22 November 2025; revised 11 March 2026; accepted 11 May 2026. Date of publication 15 May 2026; date of current version 29 May 2026.
The review of this article was arranged by Editor M. de Souza.

*Digital Object Identifier 10.1109/JEDS.2026.3693909*

# A Fast and Accurate Method for Multi-Electrode Electrostatic Lens Design

**KANGPEI YAO[1], WENTAO MA[1], HUAN HUANG[1], GANG LI[2], ZHIQING DING[1], AND JIE LIU[2,3,4]**

[1]College of Electrical and Information Engineering, Hunan University, Changsha 410082, China
[2]College of Integrated Circuits, Hunan University, Changsha 410082, China
[3]Greater Bay Area Institute for Innovation, Hunan University, Guangzhou 511300, China
[4]Yuelushan Center for Industrial Innovation, Changsha, Hunan 410082, China

CORRESPONDING AUTHOR: J. LIU (jie_liu@hnu.edu.cn)

This work was supported in part by the Yuelushan Center for Industrial Innovation Project under Grant 2025YCII0103 and Grant 2023YCII0104; in part by the National Natural Science Foundation of China under Grant 62474058 and Grant 61804049; in part by the Huxiang High Level Talent Gathering Project under Grant 2019RS1023; in part by the Technology Innovation and Entrepreneurship Funds of Hunan Province, China, under Grant 2019GK5029; and in part by the Fund for Distinguished Young Scholars of Changsha, Hunan, China, under Grant kq1905012.

**ABSTRACT** Global optimization of multi-electrode electrostatic lens systems requires thousands of electric field and trajectory computations, creating a prohibitive computational burden. Conventional volumetric solvers, such as the finite element method (FEM) and finite difference method (FDM), are accurate but slow. In contrast, fast asymptotic methods like the second-order element method (SOEM) sacrifice accuracy, particularly in off-axis regions. This paper presents an accelerated framework that combines the boundary element method (BEM) for high-precision field calculation with an adaptive Euler integration scheme for trajectory tracing. The BEM reduces dimensionality by discretizing only electrode boundaries and provides analytical field derivatives. The adaptive Euler method controls local truncation error while minimizing the number of computationally expensive field evaluations. This approach maintains full generality while achieving a 10–100× speedup in field solution and a 17× end-to-end acceleration per simulation compared to standard FDM. This performance enables practical global optimization (e.g., via genetic algorithms), reducing process duration from days to hours. The method's efficacy is validated through benchmarks and the successful design and experimental verification of a quadrupole collimator.

**INDEX TERMS** Electron optics, electrostatic lens, boundary element method (BEM), genetic algorithm, global optimization.

## I. INTRODUCTION

Global optimization of multi-electrode electrostatic lenses is a critical task for advancing the performance of electron beam equipment, including microwave tubes [1], electron beam lithography systems [2], and related technologies. Traditional design often relies on local optimization techniques like the damped least squares (DLS) method, which is prone to converging to suboptimal local minima and offers no guarantee of finding a global optimum. To overcome this fundamental limitation, global optimization heuristics such as the genetic algorithms (GAs) have been introduced to the field [3]. However, their global optimization power is counterbalanced by a prohibitive computational cost, as the optimization process requires thousands of high-fidelity calculations of electric fields and electron trajectories. This necessitates simulation methods that are both highly accurate and computationally efficient. Recent comparative studies on electron lens optimization have systematically evaluated different optimization techniques, concluding that population-based global methods such as the GAs and the particle swarm optimization (PSO) significantly outperform single-point local search methods [4].

Conventional numerical solvers, such as the finite element method (FEM) and finite difference method (FDM), are accurate but computationally intensive due to their reliance on volumetric meshing [5], [6]. This makes FEM/FDM-based GA optimization impractically slow. Accelerated methods like the second-order element method (SOEM) [7] have been developed. However, SOEM and similar expansion-based techniques suffer from significant inaccuracies, particularly

in off-axis regions. Reported errors in spherical aberration coefficients can exceed 90%. Sabouri and Perez-Martinez [8] integrated genetic algorithms with differential algebra (DA) for electrostatic lens optimization. The DA method enables rapid calculation of aberration coefficients, making the optimization process computationally efficient. Nevertheless, their foundational formalism, often based on paraxial theory, limits their applicability and accuracy for non-paraxial systems.

The Boundary Element Method (BEM) presents a compelling alternative [9], [10]. Unlike FEM/FDM, BEM only requires discretization of electrode boundaries, drastically reducing computational overhead—a key advantage recognized since early applications to electrostatic lenses [11]. Furthermore, it directly provides the electric potential and its derivatives analytically, offering superior accuracy over methods that require numerical differentiation. In this work, we leverage BEM's strengths to overcome the speed-accuracy trade-off. We combine it with an adaptive Euler method for trajectory integration, a scheme proven to achieve high precision [12]. This approach maintains full generality, being equally applicable to paraxial and non-paraxial systems.

We have conducted rigorous validation of this universal fast-computation method through comprehensive benchmarks in Section II. Furthermore, we successfully demonstrated its practical effectiveness in a GA-based optimization of a multi-electrode collimator, with results corroborated by experimental measurements, in Section III.

## II. METHODOLOGY

This section introduces the details of the BEM in part A, and the adaptive step-size particle tracking algorithm in part B.

### A. BOUNDARY ELEMENT METHOD FOR AXISYMMETRIC ELECTRIC FIELD CALCULATION

The Boundary Element Method (BEM) is a powerful numerical technique for solving the Laplace equation governing electrostatic fields in charge-free regions. The method's foundation lies in transforming the domain-governing equation into a boundary integral equation using the Green's function, which serves as the fundamental solution to the Laplace equation.

Green's function is given by $G = -1/(4\pi|\boldsymbol{r}|)$, where $\boldsymbol{r}$ represents the distance between the potential point $P\ (r_0, z_0, \theta_0)$ and the boundary element $B\ (r, z, \theta)$. It describes the relationship between the potential $u_p$ at P and the boundary potential $u_b$ as well as its normal derivative. Through the mapping between Cartesian and cylindrical coordinates, we can reduce the dimensionality of the axisymmetric three-dimensional boundary integral equation, as shown in (1).

$$ds = rdld\theta\ x = r\cos\theta\ y = r\sin\theta\ z = z$$
$$C_i \cdot u_p = \iint_S (u_b \cdot \partial G/\partial \boldsymbol{n} - G \cdot \partial u_b/\partial \boldsymbol{n}) ds$$
$$= \int_\Gamma (u_b \cdot \partial G_i/\partial \boldsymbol{n} - G_i \cdot \partial u_b/\partial \boldsymbol{n}) rdl(r, z)$$
$$G_i(r, z, r_0, z_0) = \int_0^{2\pi} G(r, z, \theta, r_0, z_0, \theta_0)\, d\theta \quad (1)$$

By utilizing elliptic integrals, we can simplify the $\theta_0 = 0$ and derive axisymmetric boundary integral equations for the electric potential [13]. The detailed derivation can be found in (2),

$$G_i = \frac{-K(f_1)}{\pi\sqrt{f_2}}$$
$$\partial G_i/\partial \boldsymbol{n} = \frac{-1}{\pi\sqrt{f_2}} \left\{ \frac{n_r}{2r} \left[ \frac{f_4}{f_3} E(f_1) - K(f_1) \right] + n_z \frac{z_0 - z}{f_3} E(f_1) \right\}$$
$$K(m) = \int_0^{\pi/2} \frac{1}{\sqrt{1 - m\sin^2 t}} dt \quad E(m) = \int_0^{\pi/2} \sqrt{1 - m\sin^2 t}\, dt$$
$$f_1 = \frac{4rr_0}{r^2 + r_0^2 + (z - z_0)^2 + 2rr_0}$$
$$f_2 = r^2 + r_0^2 + (z - z_0)^2 + 2rr_0$$
$$f_3 = r^2 + r_0^2 + (z - z_0)^2 + 2rr_0$$
$$f_4 = r_0^2 - r^2 + (z - z_0)^2 \quad (2)$$

where $C_i = 0.5$ if P lies on the smooth boundary elements and $C_i = 1$ if P lies on solution domain. $\boldsymbol{n} = (n_r, n_z)$ denotes the boundary unit normal vector $\boldsymbol{n}$.

Given that the electric field is the negative gradient of the electric potential as shown in (3), the electric field maintains the same level of accuracy as the electric potential.

A critical advantage of the BEM lies in the computation of the electric field. Given that the field is defined as the negative gradient of the potential, its components can be obtained by the analytical differentiation of the potential integrals. This approach, often implemented using computer-aided symbolic differentiation tools, ensures that the electric field calculation preserves the accuracy of the potential solution. Consequently, the BEM avoids the numerical error amplification typically associated with finite-difference approximations of the gradient, which constitutes a fundamental reason for its high accuracy in field computation. The resulting analytical expressions for the field components are complex and thus omitted here for brevity.

$$C_i \cdot E_r = -\iint_S (u_b \cdot \frac{\partial(\partial G_i/\partial \boldsymbol{n})}{\partial r} - \frac{\partial G_i}{\partial r} \cdot \partial u_b/\partial \boldsymbol{n}) ds$$
$$C_i \cdot E_z = -\iint_S (u_b \cdot \frac{\partial(\partial G_i/\partial \boldsymbol{n})}{\partial z} - \frac{\partial G_i}{\partial z} \cdot \partial u_b/\partial \boldsymbol{n}) ds \quad (3)$$

However, when the field point lies close to the source point, these integrals become singular and require specialized numerical treatment. From the axisymmetric Green's functions given by (1) and (2), one can derive the asymptotic behavior when the source point approaches the field point. The expressions show that $G_i$ contains a logarithmic

weak singularity, while $\partial G_i/\partial \boldsymbol{n}$ exhibits a strong singularity. Accurate evaluation of these singular integrals is essential for preserving the BEM's precision. Following established techniques for axisymmetric potential problems [13], we employ a hybrid numerical treatment. For integrals involving the logarithmic singularity, we use singularity subtraction: the singular part is extracted and integrated analytically using its local asymptotic expansion, while the remaining regular part is evaluated via standard Gaussian quadrature. For the strong singularity, we circumvent it using the rigid body mode method—a physical argument that a constant potential on a closed boundary produces zero net flux, allowing the singular integral to be determined indirectly from the regular off-diagonal contributions. All other integrals involve regular kernels and are computed by direct numerical integration.

### B. ELECTRON TRAJECTORY CALCULATION

The calculation of electron trajectories uses an adaptive step-size Euler method. For the trajectory $r(z)$, the Taylor expansion at $(r, z)$ is given by (4):

$$\begin{aligned} r(z) &= r'\Delta z + 0.5 \cdot r''\Delta z^2 + o(z^3) \\ r' &= v_z/v_r \\ r'' &= -\frac{q}{\gamma m_0 v_r^2}\left[E_z - E_r \cdot r' - \frac{1}{c^2}(v_z^2 E_z + v_z v_r E_r)\right] \end{aligned} \tag{4}$$

where $q$ and $m_0$ represent the charge and mass of the electron, respectively, $E_r$ and $E_z$ are the electric field intensities in two directions that can pass through the BEM, whereas $v_r$ and $v_z$ are the velocities of the electron in these two directions, and $c$ denotes the speed of light in vacuum and $\gamma$ represents the Lorentz factor.

An acceptable error e is defined, and appropriate step size is chosen to ensure that the second-order term of the Taylor expansion is smaller than this error:

$$\left|0.5 \cdot r''\Delta z^2\right| \le e \tag{5}$$

For the numerical integration of electron trajectories, we employ an adaptive step-size Euler method. This approach has been demonstrated to effectively enhance the precision of path integration in similar field-line tracing applications [8]. Its efficacy is particularly pronounced when coupled with the BEM, as the method provides direct access to highly accurate electric field values—and potentially higher-order derivatives—at any evaluation point. This enables a precise local estimation of the integration error, allowing the algorithm to dynamically optimize the step size. Consequently, the scheme maintains the local truncation error below a predefined tolerance while minimizing the number of computationally expensive field evaluations, thereby accelerating the overall solution process without compromising accuracy.

The efficiency of BEM-based trajectory integration stems from three key factors. First, unlike FEM/FDM, where field values are obtained through inexpensive interpolation, each BEM field evaluation requires computing boundary integrals—making the number of points the dominant cost. Second, high-order methods like RK4 require four field evaluations per step versus one for adaptive Euler, quadrupling the computational burden. Third, obtaining higher-order field derivatives in BEM is fundamentally difficult: the electric field (first derivatives) requires four integral kernels, and for Nth-order derivatives the kernel count grows as $2^{N+1}$. This exponential scaling renders analytical derivation intractable and numerical differentiation impractical, making high-order methods unsuitable for BEM-based trajectory calculations.

## III. RESULTS

This section demonstrates the efficiency of this method through an equal-diameter double-cylinder lens in part A and a GA-based optimization example of an electron collimating lens and further validates it through experiments in part B.

### A. SPEED AND ACCURACY TEST

To validate the superiority of the BEM in electrostatic lens simulation, we computed the potential of an equal-diameter double-cylinder lens as shown in Fig. 1. This configuration was selected because its axial potential has a known analytical expression, as shown in (6), which is derived for infinitely long cylinders. In our numerical model, this theoretical condition was approximated by setting the electrode length significantly larger than the inter-electrode gap. The computational results are shown in Fig. 2. The computational speed and accuracy of the FDM, FEM, SOEM, and BEM were compared against this benchmark, with the results shown in Fig. 3 and TABLE 1. For a fair comparison, both FDM and FEM were implemented in an axisymmetric 2D formulation consistent with the BEM framework.

$$U_z = \frac{U_1 + U_2}{2} + \frac{R}{2wz_s}(U_2 - U_1)\frac{\log(\cosh(w(z+0.5 \cdot z_s))/R)}{\cosh(w(z-0.5 \cdot z_s))/R} \tag{6}$$

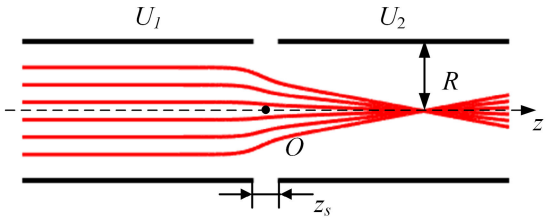


**FIGURE 1. Schematic diagram of the equal-diameter double-cylinder lens (±1 V): radius $R$ = 0.01 m, gap $z_s$ =0.001 m, $w$ = 1.32.**

The relative error of the computed axial potential is plotted against computation time for each method. BEM achieves the highest accuracy, converging to a minimum relative error of 0.016% within seconds. FDM and FEM require significantly longer computation times to reach minimum errors of 0.67% and 2.9%, respectively. SOEM, despite its speed, saturates at a much higher error of approximately 8.2% and exhibits limited convergence, confirming its inadequacy for high-precision off-axis field representation. These results

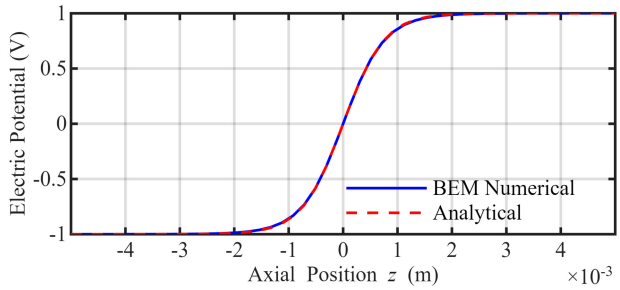


**FIGURE 2.** BEM-computed on-axis potential in an equal-diameter double-cylinder lens.

demonstrate that BEM provides the best trade-off between accuracy and efficiency.

The proposed BEM framework establishes an optimal compromise between computational efficiency and numerical precision. By employing boundary-only discretization, it reduces problem dimensionality while maintaining analytical field solution capabilities. This approach achieves accuracy comparable to refined FDM/FEM implementations while delivering 10-100× acceleration in field computation.

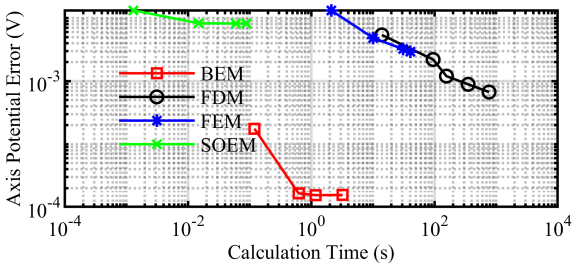


**FIGURE 3.** Accuracy and speed tests for the on-axis potential calculations of an equal-diameter double-cylinder lens via four methods, under varying mesh densities.

**TABLE 1.** Comparison of numerical methods.

| Method | Single-solution Time (s) | Minimum Relative Error | Applicable for Non-paraxial |
|---|---|---|---|
| BEM | 7.81 | 0.016% | Yes |
| FEM | 133 | 2.9% | Yes |
| FDM | 142 | 0.67% | Yes |
| SOEM | 0.520 | 8.2% | No |

For the numerical integration of electron trajectories, two distinct approaches were implemented and compared. The adaptive step-size Euler method provides first-order accuracy by utilizing a local truncation error estimate derived from the Taylor expansion of the trajectory equation. This approach dynamically adjusts the integration step size to maintain the local error below a predefined tolerance, offering computational efficiency through minimal field evaluations per step.

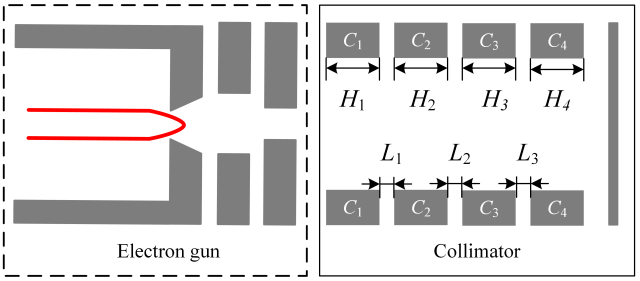


**FIGURE 4.** Experimental test subject: 1. The 2 kV electron gun consists of a hairpin cathode, a Wehnelt cup, a modulation electrode (which adjusts divergence angle of the electron gun) and an anode. 2. The four-cylinder electrode collimator.

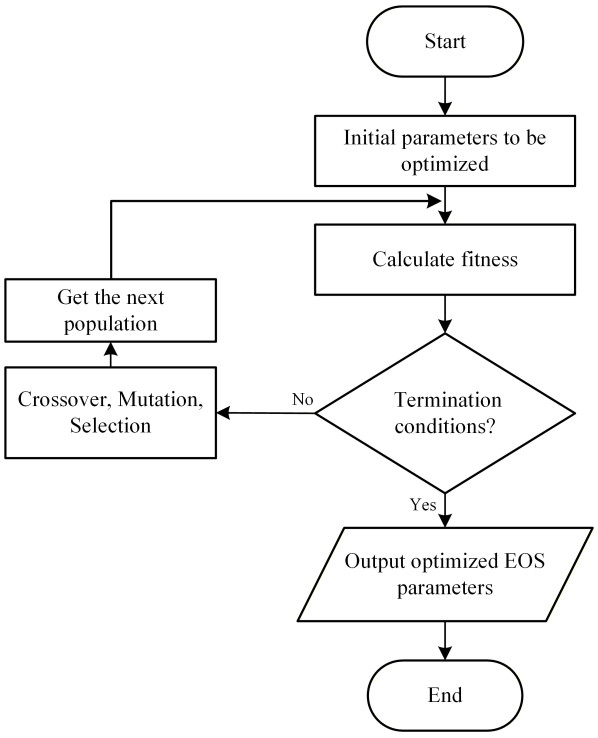


**FIGURE 5.** Genetic algorithm optimization of electron-optical system parameters.

### B. OPTIMIZATION AND EXPERIMENT

To demonstrate the practical applicability of the proposed method, we present a genetic algorithm-based optimization of a realistic non-paraxial four-electrode electron optical system, with the overall structure shown in Fig. 4.

For the electron gun region dominated by space charge effects, a specialized axisymmetric FEM solver was employed due to the limitations of BEM in handling volumetric charge distributions. The FEM solution provided critical beam parameters at the anode plane—including beam radius, divergence half-angle, and beam current—which were then used as input conditions for the BEM-based lens optimization. This approach ensures physical consistency while maintaining computational efficiency in their respective domains of applicability.

GA is a class of search and optimization techniques inspired by the principles of natural selection and genetics. GA is particularly suitable for optimizing electron optical systems, which often involve multiple parameters and highly nonlinear objective functions. The objective function landscape can be complex, causing gradient-based optimization techniques to easily converge to local optima. GAs, by contrast, explore a broader solution space through stochastic operators, thus exhibiting a greater potential for locating the global optimum. The optimization procedure generally follows Fig. 5.

The computational burden of GA-based electron optical system optimization predominantly stems from fitness function evaluations. To accelerate this process, we employ the BEM and adaptive Euler method described in Section II to efficiently compute the electron beam divergence angle. Specifically, the divergence angle is determined from ten representative electron trajectories at the working plane, enabling rapid construction of the fitness function for optimization.

In our genetic algorithm selection strategy, we employ a proportional selection method, with a crossover probability set to 0.8, mutation probability set to 0.1, and a population size of 50. The fitness function is designed to minimize beam divergence angle.

In particular, considering the practical manufacturing process, we often impose constraints on the parameters. In this design, for the seven geometric dimensions, we ensure that their range is between 1 and 10 mm with a minimum step size of 1 mm. For the four voltage parameters, we ensure their range is from −3000 to 0 V, with a minimum step size of 1 V. The divergence angle for each generation is shown in Fig. 6.

We set 11 parameters to be optimized in GA, including the seven illustrated geometric parameters and the voltages of the four collimating electrodes. After 21 generations (1050 calculations), optimization reduced the electron beam divergence from 300 mrad to 0.106 mrad. The optimized parameters can be found in TABLE 2.

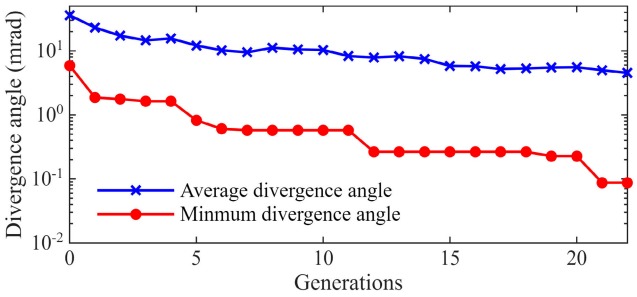


**FIGURE 6.** Optimization pathway of electron beam divergence angle using GA.

A grid convergence analysis was performed to validate the optimization results obtained from the two numerical methods. For a comparable level of accuracy (convergence

**TABLE 2.** Optimized parameter table.

| Parameter | Value | Parameter | Value | Parameter | Value |
|---|---|---|---|---|---|
| $U_{c1}$ | -1549 V | $H_1$ | 7 mm | $L_1$ | 6 mm |
| $U_{c2}$ | -1301 V | $H_2$ | 8 mm | $L_2$ | 4 mm |
| $U_{c3}$ | -1360 V | $H_3$ | 7 mm | $L_3$ | 2 mm |
| $U_{c4}$ | -914 V | $H_4$ | 6 mm | - | - |

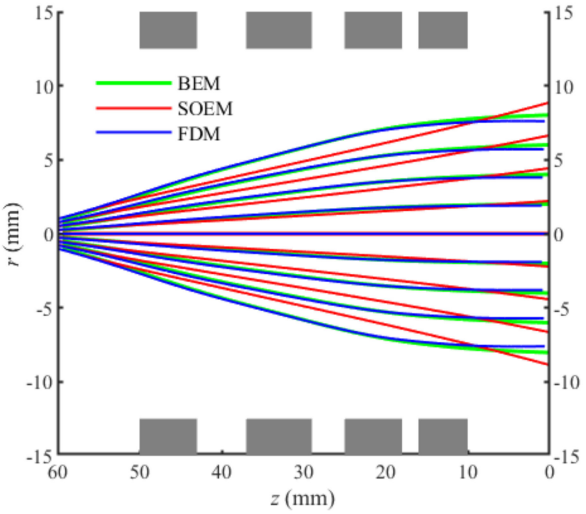


**FIGURE 7.** Simulating the collimator via the SOEM, FDM, and BEM.

error < 0.1%), BEM completes a single simulation in only 7.8 seconds—a task that requires 133 seconds using FDM, representing a 17-fold speedup. This performance gain is magnified significantly in the context of a full global optimization workflow. The FDM-based optimization necessitates approximately 41 hours to converge, whereas our BEM-driven process accomplishes the same task in just 2.1 hours. The comprehensive computational performance comparison between these algorithms is systematically presented in Fig. 8.

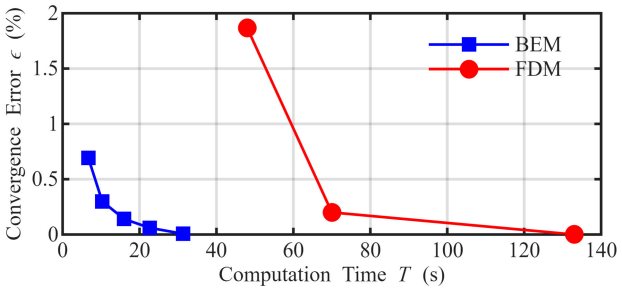


**FIGURE 8.** Convergence and computation time for BEM and FDM.

Three fundamental factors contribute to this performance difference. First, the dimensional reduction inherent in BEM's formulation—transforming the 3D boundary-value problem into a 2D integral equation—drastically reduces

the number of degrees of freedom compared to domain-discretization methods. Second, the analytical differentiation of the potential integral enables direct, high-accuracy field evaluation without the numerical error amplification typical of finite-difference gradient approximations. Third, the method's boundary-only discretization allows targeted field computation exclusively along electron trajectories, eliminating redundant volumetric calculations inherent in FDM/FEM. This combination of theoretical elegance and computational economy makes BEM particularly suitable for population-based optimization algorithms, where thousands of field evaluations are required. The reported 17× speedup per iteration, multiplied across generations, effectively transforms design cycles from days to hours, rendering previously infeasible global optimization tasks practically attainable.

Beam divergence characterization was performed using the pepper-pot method, with the experimental setup illustrated in Fig. 9. This technique employs a perforated plate containing multiple precision apertures positioned normal to the electron beam path. The resulting beamlet patterns projected onto the fluorescent screen enable accurate measurement of the beam's divergence characteristics. While the pepper-pot method provides comprehensive beam emission phase-space information, the present study focuses specifically on quantifying the total beam divergence angle. The calculation formula is (7),

$$\alpha = \overline{\arctan\left(\frac{d' - d}{2L}\right)} \tag{7}$$

where $L = 500$ mm represents the fixed distance between the pepper-pot plate and the fluorescent screen, d denotes the characteristic dimension of the aperture pattern on the pepper-pot plate, and d′ corresponds to the measured pattern dimension on the detection screen.

Experimental measurements recorded an average beam divergence angle of 0.84 mrad over the 500 mm propagation distance. This value differs from the simulated divergence of 0.106 mrad obtained through our optimization procedure. We attribute this discrepancy primarily to practical implementation constraints, including mechanical assembly tolerances that introduce component misalignment, and potential dimensional variations in the fabricated electrodes. Such deviations from the ideal axisymmetric model used in simulations can significantly alter the electrostatic field distribution, consequently affecting beam focusing characteristics. Additional contributing factors may include space charge effects at operational currents and residual electromagnetic field interference, though these were not modeled in the current simulation framework. Future work will incorporate tolerance analysis and advanced compensation techniques to bridge this simulation-experiment gap.

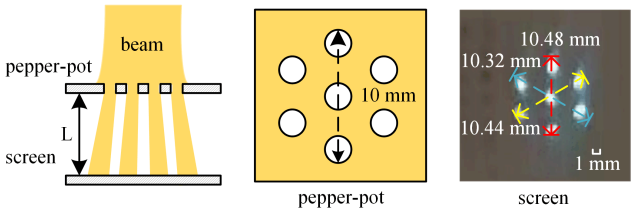


**FIGURE 9. Pepper-pot method: The electron beam passes through a pepper-pot plate and is projected onto a detection screen.**

## IV. LIMITATIONS AND FUTURE WORK

Despite the demonstrated advantages of the proposed BEM-adaptive Euler framework for axisymmetric electrostatic lens optimization, several limitations should be noted. First, the current implementation is restricted to axisymmetric geometries and does not extend to fully three-dimensional, non-axisymmetric components such as deflectors, multipoles, and aberration correctors. Second, BEM solutions exhibit accuracy degradation near electrode boundaries due to the singular nature of Green's function kernels, which manifests as non-physical field oscillations that adversely affect non-paraxial trajectory calculations. Third, the high computational cost of each BEM field evaluation makes higher-order integration schemes such as Runge-Kutta methods prohibitively expensive, motivating our deliberate choice of the adaptive Euler method as a pragmatic compromise between accuracy and efficiency.

These limitations point toward several promising research directions. The core optimization workflow is not inherently limited to axisymmetric geometries and could be extended to general 3D systems by leveraging existing mature BEM implementations such as CPO3Ds. Furthermore, incorporating Fourier series expansions into the BEM formulation offers a path to overcoming the accuracy constraints identified above: expanding the potential and its derivatives in Fourier series around the symmetry axis would provide analytical expressions for higher-order field components without additional boundary integral evaluations. This would improve field smoothness near boundaries and enable efficient high-order trajectory integration, ultimately enhancing precision for non-paraxial rays while preserving the computational efficiency required for population-based global optimization.

## V. CONCLUSION

This paper has presented an integrated BEM-adaptive Euler framework for electron optics simulation that simultaneously addresses the dual challenges of computational efficiency and physical accuracy. The methodology achieves a 10-100× acceleration in field computation compared to conventional FEM/FDM approaches while maintaining rigorous accuracy, particularly in non-paraxial regimes where asymptotic methods like SOEM show significant limitations. The quadrupole collimator case study demonstrates the framework's practical capability for global optimization of complex multi-electrode systems, with experimental measurements confirming the

fundamental validity of the approach. By effectively decoupling the traditional trade-off between computational speed and numerical precision in electron optical simulation, this work establishes a foundation for computationally feasible design optimization of advanced electron optical systems that was previously constrained by numerical limitations. The methodology's boundary-only formulation and analytical field solution provide inherent advantages for iterative optimization workflows, suggesting potential applications across a broader range of charged particle beam design problems.

## REFERENCES

[1] J. Eichmeier and M. Thumm, *Vacuum Electronics: Components and Devices*. Berlin, Germany: Springer, 2008.

[2] V. Kuiper et al., "Mapper: High throughput maskless lithography," in *Proc. 25th Eur. Mask Lithography Conf.*, vol. 7470, Jan. 2009, pp. 1–5.

[3] A. Akhatov, F. Nazarov, M. Nurmamatov, and S. Sariyev, "Genetic algorithm application technology in multi-parameter optimization problems," *AIP Conf. Proc.*, vol. 3244, Nov. 2024, Art. no. 030025, doi: 10.1063/5.0242074.

[4] N. H. M. Nezhad, M. G. Niasar, C. W. Hagen, and P. Kruit, "Comparison of different optimization techniques in electron lens design," in *Proc. 9th Int. Conf. Optim. Appl. (ICOA)*, Oct. 2023, pp. 1–5, doi: 10.1109/icoa58279.2023.10308847.

[5] N. Hesam Mahmoudi Nezhad, M. Ghaffarian Niasar, A. Mohammadi Gheidari, C. W. Hagen, and P. Kruit, "Multi-electrode lens optimization using genetic algorithms," *Int. J. Modern Phys. A*, vol. 34, no. 36, Dec. 2019, Art. no. 1942020, doi: 10.1142/s0217751x1942020x.

[6] C. X. Gu, M. Q. Wu, G. Lin, and L. Y. Shan, "The global optimization design for electron emission system using genetic algorithms," *Nucl. Instrum. Methods Phys. Res. A, Accel. Spectrom. Detect. Assoc. Equip.*, vol. 519, nos. 1–2, pp. 90–95, Feb. 2004, doi: 10.1016/j.nima.2003.11.126.

[7] N. Hesam Mahmoudi Nezhad, M. Ghaffarian Niasar, A. Mohammadi Gheidari, P. Kruit, and C. W. Hagen, "Multiple criteria optimization of electrostatic electron lenses using multiobjective genetic algorithms," *J. Vac. Sci. Technol. B, Nanotechnol. Microelectronics: Mater., Process., Meas., Phenomena*, vol. 39, no. 6, Dec. 2021, Art. no. 062605, doi: 10.1116/6.0001274.

[8] A. Sabouri and C. S. Perez-Martinez, "Design of electrostatic lenses through genetic algorithm and particle swarm optimisation methods integrated with differential algebra," *Ultramicroscopy*, vol. 266, Dec. 2024, Art. no. 114024, doi: 10.1016/j.ultramic.2024.114024.

[9] F. H. Read and N. J. Bowring, "The CPO programs and the BEM for charged particle optics," *Nucl. Instrum. Methods Phys. Res. A, Accel. Spectrom. Detect. Assoc. Equip.*, vol. 645, no. 1, pp. 273–277, Jul. 2011, doi: 10.1016/j.nima.2010.12.163.

[10] J. S. Loyd and D. A. Gregory, "Precision enhancement in boundary element methods with application to electron optics," *Microscopy*, vol. 65, no. 4, pp. 325–336, Aug. 2016, doi: 10.1093/jmicro/dfw012.

[11] J. Ximen and D. Li, "Three-dimensional boundary-element method for analyzing nonrotationally symmetric perturbations in electrostatic lenses," *J. Appl. Phys.*, vol. 67, no. 4, pp. 1643–1649, Feb. 1990, doi: 10.1063/1.345631.

[12] J. Liu, J. Zou, J. Tian, J. Yuan, and X. Ma, "An accurate adaptive method for drawing 2-D electric lines of force," in *Proc. 8th Int. Symp. Antennas, Propag. EM Theory*, Nov. 2008, pp. 792–795, doi: 10.1109/isape.2008.4735335.

[13] L. J. Gray, M. Garzon, V. Mantic, and E. Graciani, "Galerkin boundary integral analysis for the axisymmetric Laplace equation," *Int. J. Numer. Methods Eng.*, vol. 66, no. 13, pp. 2014–2034, Jun. 2006, doi: 10.1002/nme.1613.